Diffusive Transport Enhanced by Thermal Velocity Fluctuations

Aleksandar Donev,[1,*] John B. Bell,[2] Anton de la Fuente,[3] and Alejandro L. Garcia[3]

[1] *Courant Institute of Mathematical Sciences, New York University, New York, NY 10012*
[2] *Center for Computational Science and Engineering, Lawrence Berkeley National Laboratory, Berkeley, CA, 94720*
[3] *Department of Physics, San Jose State University, San Jose, California, 95192*

We study the contribution of advection by thermal velocity fluctuations to the effective diffusion coefficient in a mixture of two indistinguishable fluids. We find good agreement between a simple fluctuating hydrodynamics theory and particle and finite-volume simulations. The enhancement of the diffusive transport depends on the system size L and grows as $\ln(L/L_0)$ in quasi two-dimensional systems, while in three dimensions it scales as $L_0^{-1}-L^{-1}$, where L_0 is a reference length. Our results demonstrate that fluctuations play an important role in the hydrodynamics of small-scale systems.

Thermal fluctuations in non-equilibrium systems in which a constant (temperature, concentration, velocity) gradient is imposed externally exhibit remarkable behavior compared to equilibrium systems [1]. The solution of the linearized equations of fluctuating hydrodynamics shows that concentration and density fluctuations exhibit long-ranged correlations in the presence of a macroscopic concentration gradient $\boldsymbol{\nabla} c$ [1–3]. The enhancement of large-scale (small wavenumber) concentration fluctuations is dramatic during the early stages of diffusive mixing between initially phase-separated fluids. These *giant fluctuations* [4–6] during free diffusive mixing have been measured using light scattering and shadowgraphy techniques [4, 5, 7], finding good but imperfect agreement with theoretical predictions.

The giant fluctuation phenomenon arises because of the appearance of long-ranged correlations between concentration and velocity fluctuations in the presence of a concentration gradient. It has been predicted that these correlations give rise to fluctuation-renormalized transport coefficients [3, 8**?**]; however, the predicted enhancement of transport at hydrodynamic scales has not yet been computationally observed. In particular, it is important to understand how the effective transport coefficients depend on the length scale of observation.

In this Letter we consider diffusion in a mixture of identical but labeled (as components 1 and 2) fluids [9] enclosed in a box of size $L_x \times L_y \times L_z$, in the absence of gravity. Periodic boundary conditions are applied in the x (horizontal) and z (depth) directions, while the top and bottom boundaries are impermeable constant-temperature walls. A concentration gradient $\nabla\bar{c} = (c_T - c_B)/L_y$ is imposed along the y axes by enforcing a constant concentration c_T at the top wall and c_B at the bottom wall. Because the fluids are indistinguishable, concentration is *passively* transported by thermal fluctuations.

Since species are not changed in particle collisions, the diffusive transport of concentration $c = \rho_1/\rho$ can only occur via advective motion of the particles, where ρ denotes the mass density. The mass flux for a given species is therefore equal to the momentum density for particles of that species. At steady state the particles of a given species have a non-zero macroscopic momentum density $\bar{\boldsymbol{j}}_1 = \bar{\rho}_1\bar{\boldsymbol{v}}_1 = -\bar{\rho}\chi\,(\boldsymbol{\nabla}\bar{c})$, where χ is the mass diffusion coefficient [10]. The local fluctuations around the macroscopic mean, $\rho_1 = \bar{\rho}_1 + \delta\rho_1$ and $\boldsymbol{v}_1 = \bar{\boldsymbol{v}}_1 + \delta\boldsymbol{v}_1$, can also make a non-trivial contribution to the average mass flux if they are correlated,

$$\langle \boldsymbol{j}_1 \rangle = \langle \rho_1 \boldsymbol{v}_1 \rangle = -\bar{\rho}\chi\,(\boldsymbol{\nabla}\bar{c}) + \langle (\delta\rho_1)\,(\delta\boldsymbol{v}_1)\rangle. \qquad (1)$$

At mesoscopic scales the hydrodynamic behavior of fluids can be described with the Landau-Lifshitz Navier-Stokes (LLNS) equations of fluctuating hydrodynamics [1, 11]. The incompressible isothermal LLNS equations for a mixture of two indistinguishable fluids are

$$\partial_t \boldsymbol{v} = -\boldsymbol{\nabla}\pi - \boldsymbol{v}\cdot\boldsymbol{\nabla}\boldsymbol{v} + \nu\boldsymbol{\nabla}^2\boldsymbol{v} + \boldsymbol{\nabla}\cdot(A_v\,\boldsymbol{\mathcal{W}}), \qquad (2)$$

$$\partial_t c = -\boldsymbol{v}\cdot\boldsymbol{\nabla}c + \chi\boldsymbol{\nabla}^2 c + \boldsymbol{\nabla}\cdot(A_c\,\widetilde{\boldsymbol{\mathcal{W}}}) \qquad (3)$$

where η is the viscosity and $\nu = \eta/\rho$, and the pressure π enforces $\boldsymbol{\nabla}\cdot\boldsymbol{v} = 0$. The stochastic fluxes are white-noise random Gaussian tensor $\boldsymbol{\mathcal{W}}$ and vector $\widetilde{\boldsymbol{\mathcal{W}}}$ fields, with amplitudes $A_v^2 = 2\eta k_B T/\rho^2$ and $A_c^2 = 2m\chi c(1-c)/\rho$ determined from the fluctuation-dissipation principle, where m is the fluid particle mass.

In addition to the usual Fickian contribution, the diffusive flux in (3) includes advection by the fluctuating velocities $\boldsymbol{v} = \delta\boldsymbol{v}$,

$$-\boldsymbol{v}\cdot\boldsymbol{\nabla}\,(\delta c) + \chi\boldsymbol{\nabla}^2\,(\delta c) = \boldsymbol{\nabla}\cdot\left[-\,(\delta c)\,(\delta\boldsymbol{v}) + \chi\boldsymbol{\nabla}\,(\delta c)\right],$$

which is a quadratic function of the fluctuations. To leading order, the advective contribution to the average diffusive mass flux is approximated using the solution of the *linearized* equations,

$$-\langle (\delta c)\,(\delta\boldsymbol{v})\rangle \approx -\langle (\delta c)\,(\delta\boldsymbol{v})\rangle_{\text{linear}} = (\Delta\chi)\,\boldsymbol{\nabla}\bar{c}.$$

The *effective* diffusion coefficient $\chi_{\text{eff}} = \chi + \Delta\chi$ thus includes an *enhancement* $\Delta\chi$ due to thermal velocity fluctuations, in addition to the *bare* diffusion coefficient χ.

The solution to the linearized form of (2,3) in the Fourier domain [3, 12] shows that the concentration fluctuations and the fluctuations of velocity parallel to the gradient develop long ranged correlations,

$$\mathcal{S}_{c,v_\parallel} = \langle (\widehat{\delta c})(\widehat{\delta v_\parallel}^{\star})\rangle = -\frac{k_B T}{\rho(\nu+\chi)k^2}\left(\sin^2\theta\right)\,\nabla\bar{c}. \qquad (4)$$

where θ is the angle between $\boldsymbol{k}$ and $\boldsymbol{\nabla}\bar{c}$, $\sin^2\theta = k_\perp^2/k^2$,

a hat denotes the Fourier transform, and star denotes the complex conjugate. The power-law divergence for small k indicates long ranged correlations between δc and $\delta v_\parallel$, and is the cause of both the giant fluctuation phenomenon and the diffusion enhancement. As seen from (1), the actual correlation that determines the diffusion enhancement is $\mathcal{S}_{\rho_1,v_\parallel^{(1)}} = \langle(\widehat{\delta c})(\widehat{\delta v_\parallel^{(1)}})^\star\rangle \approx \bar{\rho}\mathcal{S}_{c,v_\parallel}$.

We verify the predictions of fluctuating hydrodynamics by using the Direct Simulation Monte Carlo (DSMC) particle algorithm [13]. Previous careful measurements of transport coefficients in DSMC have been limited to quasi one-dimensional simulations [14]. The effect we are exploring here does not appear in one dimension as it arises because of the presence of vortical modes in the fluctuating velocities. We have performed DSMC calculations for an ideal hard-sphere gas with molecular diameter $\sigma = 1$ and molecular mass $m = 1$, at an equilibrium density of $\rho_0 = 0.06$, with the temperature kept at $k_B T_0 = T_0 = 1$ via thermal collisions with the top and bottom walls. Each DSMC particle represents a single hard sphere so the mean free path is $\lambda = 3.75$ and the mean free collision time is $\tau = 2.35$. The DSMC time step was chosen to be $\Delta t = \tau/2$, and the collision cell size is either $\Delta x_c = \lambda$ or $\Delta x_c = 2\lambda$. A uniform concentration gradient along the vertical (y) direction is implemented by randomly selecting the species of particles to be one with probability $c_{T/B}$ if they collide with the top/bottom wall. Hydrodynamic quantities such as velocity and concentration are calculated from the particle data by using a grid of $N_x \times N_y \times N_z$ *sampling* or *hydrodynamic cells*, each of volume $\Delta V = \Delta x\, \Delta y\, \Delta z$, and a discrete Fourier transform is used to obtain static structure factors.

To compare the prediction (4) to results from particle simulations, we have converted the *continuum* static structure factor $\mathcal{S}_{c,v_\parallel}(\boldsymbol{k})$ into a *discrete* structure factor $S_{c,v_\parallel}(\boldsymbol{\kappa})$ for finite-volume averages of the continuum fields, where the wavenumbers $\boldsymbol{\kappa} \in \mathbb{Z}^3$ index the discrete set of wavevectors compatible with periodicity [12]. In Fig. 1 we compare the theoretical prediction for $\bar{\rho}S_{c,v_\parallel}(\boldsymbol{\kappa})$ to DSMC results for the discrete structure factor $\mathcal{S}_{\rho_1,v_\parallel^{(1)}}$. Similar results are obtained for two different sizes of the DSMC collision cells [12], $\Delta x_c = 2\lambda$ and $\Delta x_c = \lambda$, verifying that the details of the microscopic collision dynamics do not affect the mesoscopic hydrodynamic behavior.

It is expected that compressibility effects would affect $\mathcal{S}_{\rho_1,v_\parallel^{(1)}}$. In order to construct a theoretical prediction, however, one must not only include the effect of compressibility but also replace the "one-fluid" approximation with a corresponding "two-fluid" compressible hydrodynamic theory [10]. As Fig. 1 demonstrates, the incompressible isothermal theory for $\bar{\rho}S_{c,v_\parallel}$ can be used as a *proxy* for $\mathcal{S}_{\rho_1,v_\parallel^{(1)}}$ in order to construct theoretical predictions for the diffusion enhancement.

The mass flux due to advection by the fluctuating velocities can be approximated using (4) as

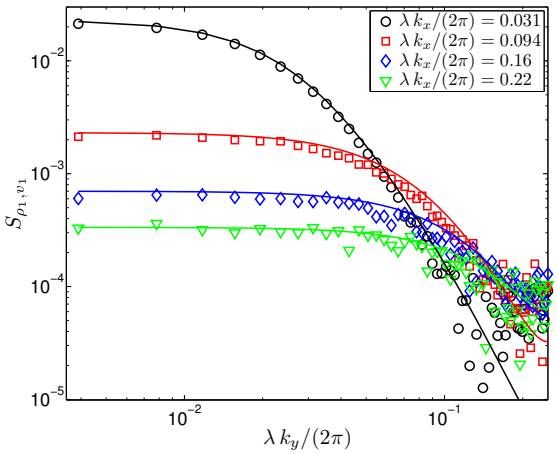

Figure 1: (Color online) Discrete structure factor $\mathcal{S}_{\rho_1,v_\parallel^{(1)}}$ from quasi two-dimensional DSMC runs with $L_x = 64\lambda$, $L_y = 512\lambda$ and $L_z = 2\lambda$, for several wavenumbers $k_x = \kappa_x \cdot 2\pi/L_x$ (see legend), compared to the discrete equivalent of the continuum prediction (4) (solid lines of the same color). Note that for a fixed k_x we expect the structure factor to decay as k_y^{-4}.

$$\langle(\delta c)\,(\delta \boldsymbol{v})\rangle_{\text{linear}} = (2\pi)^{-3} \int_{\boldsymbol{k}} \mathcal{S}_{c,\boldsymbol{v}}\,(\boldsymbol{k})\; d\boldsymbol{k}, \tag{5}$$

giving an estimate of the diffusion enhancement [3, 12]

$$\Delta\chi = \frac{k_B T}{(2\pi)^3 \rho\,(\chi+\nu)} \int_{\boldsymbol{k}} \left(\sin^2\theta\right) k^{-2}\, d\boldsymbol{k}. \tag{6}$$

Because of the k^{-2}-like behavior, the integral over all $\boldsymbol{k}$ above diverges unless one imposes [3] a lower bound, $k_{\min} \sim 2\pi/L$ in the absence of gravity, *and* a phenomenological cutoff $k_{\max} \sim \pi/L_{\text{mol}}$ for the upper bound, where L_{mol} is an ad-hoc "molecular" length scale.

For a quasi two-dimensional system, $L_z \ll L_x \ll L_y$, we can replace the integral over k_z with $2\pi/L_z$ and integrate over all k_y. This leads to an average total diffusive flux that grows logarithmically with the width L_x for a fixed height L_y [12],

$$\chi_{\text{eff}}^{(2D)} \approx \chi + \frac{k_B T}{4\pi\rho(\chi+\nu)L_z} \ln\frac{L_x}{L_0}, \tag{7}$$

where $L_0 > 2L_{\text{mol}}$ is the *reference* width at which the "bare" diffusion coefficient is measured. Within the phenomenological perturbative theory L_0 is an arbitrary (mesoscopic) length scale, and simply defines $\chi = \chi_{\text{eff}}(L_x = L_0)$. For comparison between the particle simulations and the theory we use $L_0 = 16\lambda$. When the system width becomes comparable to the height, boundaries will intervene and for $L_x \gg L_y$ the effective diffusion coefficient must become a constant, which is predicted to be a logarithmically-growing function of L_y in two dimensions. The same coefficient in front of $\ln L_x$ as in (7) is obtained when the integral over k_x is replaced by a discrete sum over the wavenumbers consistent with periodicity, $k_x = \kappa_x \cdot 2\pi/L_x$, $\kappa_x \in \mathbb{Z}$ [12].

In three dimensions, $L_x = L_z = L \ll L_y$, χ_{eff} con-

verges as $L \to \infty$ to the macroscopic diffusion coefficient,

$$\chi_{\rm eff}^{(3D)} \approx \chi + \frac{\alpha\, k_B T}{\rho(\chi+\nu)}\left(\frac{1}{L_0}-\frac{1}{L}\right), \qquad (8)$$

but for a finite system the effective diffusion coefficient is reduced by an amount $\sim L^{-1}$ due to the truncation of the velocity fluctuations by the confining walls. Calculating the exact value of α requires performing a sum over κ_x and κ_z instead of integrals over k_x and k_z, as we have done numerically [12]. The numerical results suggest that, as in two dimensions, the difference in $\chi_{\rm eff}^{(3D)}$ between two systems attains a finite value as $L_{\rm mol} \to 0$, justifying (8) for $(L_0, L) \gg L_{\rm mol}$.

In particle simulations, we calculate the *effective* diffusion coefficient $\chi_{\rm eff}$ from the momentum density of one of the species (denoted either with a subscript or with a parenthesis superscript) along the vertical direction,

$$\langle j_\parallel^{(1)} \rangle = \langle \rho_1 v_\parallel^{(1)} \rangle = \rho_0 \chi_{\rm eff} \frac{\bar{c}_T - \bar{c}_B}{L_y - \Delta y} \approx \rho_0 \chi_{\rm eff} \left(\nabla \bar{c}\right), \quad (9)$$

where we measure $\bar{c}_T$ and $\bar{c}_B$ in the top and bottom layer of sampling cells (whose centers are a distance $L_y - \Delta y$ from each other) to empirically account for the small concentration slip in DSMC. Numerical experiments have verified that $\langle j_\parallel^{(1)} \rangle$ matches the flux obtained from counting the average number of color flips at the top or bottom walls. Furthermore, the results verify that $\langle j_\parallel^{(1)} \rangle$ is linear in the gradient $\nabla \bar{c}$, and that $\bar{c}_{T/B}$ are essentially independent of the system dimensions.

The traditional definition of a "renormalized" diffusion coefficient [8**?**] as the macroscopic limit of $\chi_{\rm eff}$, only works in three dimensions and is not very useful for confined systems. Instead, for each sampling cell, we define a *locally renormalized* diffusion coefficient χ_0 via

$$\langle \rho_1 \rangle \langle v_\parallel^{(1)} \rangle = \langle \rho_1 \rangle \langle j_\parallel^{(1)}/\rho_1 \rangle = \bar{\rho} \chi_0 \left(\nabla \bar{c}\right), \qquad (10)$$

where we have accounted for the fact that the macroscopic concentration profile $\bar{c}(y)$ may depend on y. In fact, such a dependence is observed in the particle simulations, and we have approximated the local concentration gradient $d\bar{c}/dy$ by a numerical derivative of a polynomial of degree five fit to $\bar{c}(y)$. We have empirically observed that χ_0 is independent of y, except for a boundary layer close to the top and bottom walls [12]. This is an important finding, since (10) is a constitutive model that is assumed to hold not just at the macroscale but also at the mesoscale, notably, χ_0 is an input parameter for fluctuating hydrodynamics finite-volume solvers [15].

Figure 2a shows how $\chi_{\rm eff}$ and χ_0 change as the width of the system L_x is increased while keeping the height L_y fixed for two different quasi two-dimensional DSMC systems. For System A, the DSMC collision cells are cubes of side $\Delta x_c = 7.5 = 2\lambda$, while each sampling cell contains $2 \times 2 \times 1$ collision cells, or $N_p = 101$ particles on average. The height of the box is $L_y = 256\lambda = 960$ and the imposed concentrations at the walls are $c_B = 0.25$ and $c_T = 0.75$. For System B, the sampling cells are twice as large, $4 \times 4 \times 1$ collision cells each, and the system height is $L_y = 512\lambda = 1920$. We obtain similar results using a factor of two smaller collision cells (not shown). For the quasi two-dimensional systems, the thickness is $L_z = 7.5 = 2\lambda$ and there is only one DSMC collision cell along the z direction. Figure 2a shows that $\chi_{\rm eff}$ grows like $\ln L_x$, with a slope that is well-predicted by Eq. (7). For widths larger than about 8 mean free paths, χ_0 becomes constant and rather similar to the Chapman-Enskog kinetic theory prediction. Note that χ_0 is not a fundamental material constant and in fact depends on the shape of the sampling cells, notably, it grows as the sampling cell size is enlarged.

In Fig. 2b we show results from three dimensional DSMC simulations, in which the system width (x) and depth (z) directions are equivalent, $L_z = L_x = L$, and the rest of the parameters are as for System A. Similar behavior is seen as in two dimensions, except that now the effective diffusion grows as $-L^{-1}$ and saturates to a constant value for large L, assuming that $L_y \gg L$.

The predictions of the simplified fluctuating hydrodynamic theory, Eqs. (7) and (8), are shown in Figs. 2 and are seen to be in very good agreement with the particle simulations for intermediate L_x. However, recall that the incompressible isothermal theory assumed that L_y is essentially infinite and thus in two dimensions $\chi_{\rm eff}$ grows unbounded in the macroscopic limit. Yet when $L_x \gg L_y$, $\chi_{\rm eff}$ must saturate to a constant value, and the particle data shown in Fig. 2a shows measurable deviations from the simple theory for $L_x \gtrsim L_y/2$. One can extend the theoretical calculations to account for the hard wall boundary conditions in the y direction [1], however, such a calculation is non trivial. Instead, we have used the finite-volume solver developed in Ref. [15] to solve the LLNS non-linear system of SPDEs for the same system dimensions as in the particle simulations. To minimize the effect of nonlinearities in the SPDE solver, we artificially reduce the amplitude of the noise by some factor $\epsilon \ll 1$, but then scale all correlations by ϵ^{-2} [12]. The results, shown in Fig. 2, are in excellent agreement with the particle simulations for the larger system sizes.

In finite-volume solvers, the spacing of the computational grid plays the equivalent of the cutoff length $L_{\rm mol}$, and therefore $\chi_{\rm eff}$ depends on the grid spacing. We have added a constant to the effective diffusion coefficient obtained from SPDE runs so as to match $\chi_{\rm eff}$ from the particle simulations for $L_x = L_0 = 16\lambda$. This correction essentially renormalizes χ_0 based on the size of the finite-volume hydrodynamic cells. One can think of χ_0 as the physical-space equivalent of the wavenumber-dependent diffusion coefficient $\chi\left(\boldsymbol{k}, \omega = 0\right)$ commonly used in linear response theories [8, 9]. Theoretical predictions [12] for χ_0 indicate that χ_0 only includes "sub-grid" contributions, from wavenumbers larger than $2\pi/\Delta x$. Thus χ_0 stops increasing once the system becomes substantially larger than the size of the sampling cell. The bare diffu-

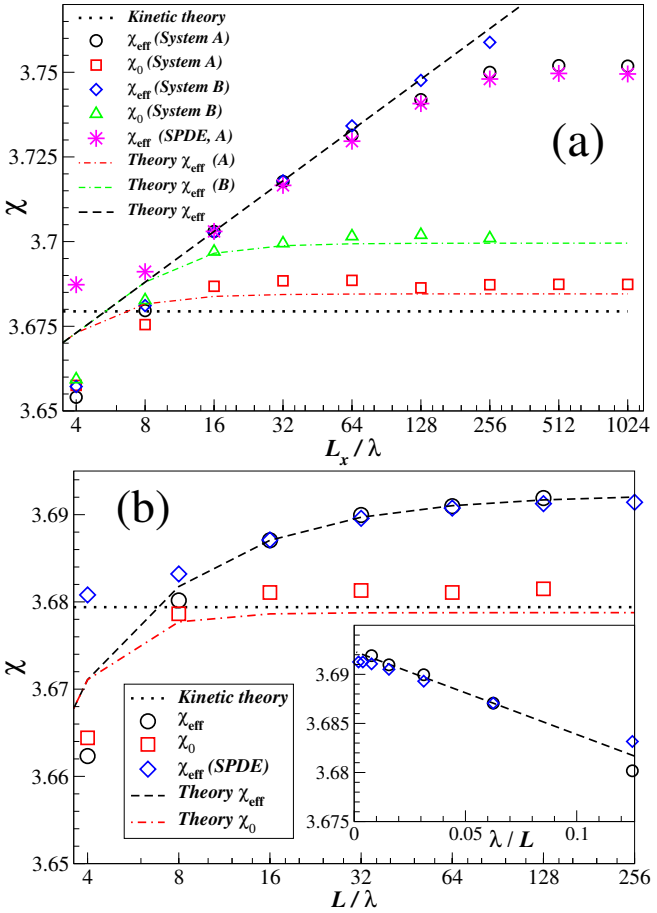

Figure 2: (Color online) (*Panel a*) The effective $\chi_{\rm eff}$ and the renormalized χ_0 diffusion coefficients as a function of the width of the system L_x in two dimensions. Numerical results for System A (DSMC and SPDE) and System B (DSMC) are shown with symbols (see legend). The error bars for all of the simulation data are comparable or smaller than the size of the symbols. The theoretical predictions [12] are evaluated numerically and shown with lines. (*Panel b*) Same as panel (a) but in three dimensions. The inset highlights the L^{-1} behavior.

sion coefficient χ in the theory and SPDE calculations is adjusted so that for $L_x = L_0 = 16\lambda$ the effective diffusion is the same as that measured in the particle simulations.

Previously-studied corrections to the bare or molecular transport coefficients due to the tail of the velocity autocorrelation function (VACF) [2], hydrodynamic interactions with periodic images of a given particle [16], and the contribution due to advection by thermal velocity fluctuations [3, 8] studied here, are all the same physical phenomenon simply calculated through different theoretical approaches, all of which are *equivalent* because of linearity [12] . In three dimensions, simple estimates indicate that the contribution of fluctuations to the macroscopic diffusion coefficient are small compared to molecular effects for gases but can be significant for liquids [12]. However, the logarithmic divergence in (7) means that $\Delta\chi \gg \chi$ for sufficiently large (quasi) two-dimensional systems, requiring the inclusion of higher order corrections in the theory. At present, reaching the system width L_x where $\Delta\chi \sim \chi$ is difficult with DSMC simulations, but it may be accessible to finite-volume SPDE solvers or experiments [6].

Our results conclusively demonstrate that the advection by thermal velocity fluctuations affects the *mean* transport in nonequilibrium finite systems. Theoretical modeling of finite systems at the nano or microscale thus requires including nonlinear hydrodynamic fluctuations. The advantage of fluctuating hydrodynamics is that it is simple, and it can take into account the proper boundary conditions and exact geometry, especially if a numerical SPDE solver is used. Furthermore, other effects such as gravity, temperature variations, or time dependence, can easily be included. However, a proper fully-nonlinear theory has yet to be developed, and requires detailed understanding of the role of the necessary large wavenumber cutoffs (regularizations). Future work should verify the predictions of fluctuating hydrodynamics for the effect of fluctuations on diffusive transport in spatially nonuniform systems.

We thank Berni Alder, Doriano Brogioli, Jonathan Goodman and Eric Vanden-Eijnden for informative discussions. This work was supported by the DOE Applied Mathematics Program (DE-AC02-05CH11231).

* Electronic address: donev@courant.nyu.edu

[1] J. M. O. D. Zarate and J. V. Sengers, *Hydrodynamic fluctuations in fluids and fluid mixtures* (Elsevier, 2006).
[2] J. R. Dorfman, T. R. Kirkpatrick, and J. V. Sengers, Annual Review of Physical Chemistry **45**, 213 (1994), ISSN 0066-426X.
[3] D. Brogioli and A. Vailati, Phys. Rev. E **63**, 12105 (2000).
[4] A. Vailati and M. Giglio, Nature **390**, 262 (1997).
[5] F. Croccolo, D. Brogioli, A. Vailati, M. Giglio, and D. S. Cannell, Phys. Rev. E **76**, 041112 (2007).
[6] D. Brogioli, ArXiv e-prints (2011), 1103.4763.
[7] A. Vailati, R. Cerbino, S. Mazzoni, C. J. Takacs, D. S. Cannell, and M. Giglio, Nature Communications **2**, 290 (2011).
[8] D. Bedeaux and P. Mazur, Physica **73**, 431, and **75**, 79, (1974).
[9] W. Wood and J. Erpenbeck, J. Stat. Phys. **27**, 37 (1982).
[10] E. Goldman and L. Sirovich, Physics of Fluids **10**, 1928 (1967).
[11] L. Landau and E. Lifshitz, *Fluid Mechanics*, (Pergamon Press, Oxford, England, 1959).
[12] A. Donev, A. L. Garcia, A. de la Fuente, and J. B. Bell, ArXiv e-print 1103.5244 (2011).
[13] G. Bird, *Molecular Gas Dynamics and the Direct Simulation of Gas Flows* (Clarendon, Oxford, 1994).
[14] D. J. Rader, M. A. Gallis, J. R. Torczynski, and W. Wagner, Physics of Fluids **18**, 077102 (2006).
[15] A. Donev, E. Vanden-Eijnden, A. L. Garcia, and J. B. Bell, CAMCOS **5**, 149 (2010).
[16] I. Yeh and G. Hummer, J. Phys. Chem. B **108**, 15873 (2004).